

Broadband Proton Decoupling for In Vivo Brain Spectroscopy in Humans

Peter B. Barker,^{1,2*} Xavier Golay,^{1,2} Dmitri Artemov,¹ Ronald Ouwerkerk,¹ Mari A. Smith,³ and A.J. Shaka³

A new decoupling sequence, PBAR, is described for broadband heteronuclear decoupling in vivo in humans at 1.5T. The sequence uses non-adiabatic, frequency- and amplitude-modulated inversion pulses designed to minimize decoupling sidebands at low applied γB_2 RF field levels and to cover only the narrow range of resonance offsets encountered in practice. The offset dependence of the decoupling efficiency of PBAR is demonstrated and compared to the conventional WALTZ-4 sequence. At the same average power levels, PBAR had slightly reduced bandwidth but significantly less intense decoupling sidebands. Applications of PBAR are shown in vivo in the human brain both for ^{31}P and natural abundance ^{13}C spectroscopy using volume decoupling coils. The PBAR sequence allows whole brain $\{^1\text{H}\}$ - ^{13}C decoupling to be performed at 1.5T with a standard head coil within FDA guidelines for RF power deposition. *Magn Reson Med* 45:226–232, 2001. © 2001 Wiley-Liss, Inc.

Key words: decoupling; broadband; spectroscopy; in vivo; carbon-13; phosphorus-31; brain

In vivo spectroscopy of nuclei such as carbon-13 (^{13}C) and phosphorus-31 (^{31}P) benefits from the application of broadband proton decoupling (1–4). Removal of heteronuclear proton couplings improves both spectral resolution and sensitivity by collapsing multiplets into single lines. In addition, pre-irradiation of protons provides additional sensitivity enhancement through the nuclear Overhauser effect (NOE). For phosphorus-31 spectroscopy in vivo, broadband proton decoupling particularly improves spectral resolution in the phosphomonoester and phosphodiester regions of the spectrum, allowing resolution of individual phosphoester compounds which are of key significance in experimental cancer studies (5). However, decoupling over the full range of proton chemical shifts (broadband decoupling) in vivo is a significant problem because of the low B_2 field strengths available with large head or body coils when using safe RF power levels (specific absorption rate (SAR) within FDA guidelines). For these reasons, previous studies of ^{13}C metabolism in the human brain have been limited to the use of surface coils for proton decoupling (1,2,4), which allows only partial brain coverage and is usually confined to the occipital-parietal region. For whole-brain spectroscopic im-

aging studies of ^{13}C metabolism in the human brain, artifact-free decoupling sequences are required to be compatible with volume head coils, which should be used both for broadband proton decoupling and ^{13}C acquisition.

Numerous broadband heteronuclear decoupling sequences have been developed for applications in conventional high-resolution NMR (3,6–13). However, there are significant differences between the decoupling requirements for in vivo NMR and high-resolution NMR. Some factors are more favorable in vivo: for instance, lower magnet field strengths result in a reduced decoupling bandwidth, and linewidths in vivo are broader than in high-resolution NMR, so a larger scaling factor (λ) (14) is acceptable. For example, it is possible to use the WALTZ-4 sequence in vivo as opposed to WALTZ-16, which has a much better scaling factor (and is therefore extensively used in high-resolution NMR) (9). However, a major problem for in vivo decoupling in humans is that very limited B_2 field strengths are available within admissible SAR levels. The use of low B_2 fields is a problem since the intensity of artifacts such as cycling sidebands (15) increases inversely with the square of the B_2 field strength; decoupling cycles become extremely long, and hence performance degrades (14). In addition, sideband spacing is the inverse of the cycle time, so long cycle times lead to dense, intense sidebands. With low B_2 fields it may also be difficult to maintain the adiabatic condition for adiabatic decoupling sequences (3,11–13). In this work, we describe a new broadband decoupling sequence for in vivo decoupling applications using frequency swept inversion pulses that are specifically designed for low-level (as opposed to wide band) applications. The performance of the sequence is compared to WALTZ-4 decoupling, and is demonstrated in vivo in the human brain and foot for both natural abundance ^{31}P and ^{13}C spectroscopy. The sequence can be used with volume head-coils and should therefore be suitable for future applications in whole-brain spectroscopic imaging studies.

METHODS AND MATERIALS

The starting point of the sequence design was the selection of a 180° inversion pulse. Since sideband intensity is a function of both the length of the sequence and the quality of inversion, for in vivo applications with low B_2 fields a short pulse element with excellent inversion properties is required. For these experiments, therefore, we chose a numerically-optimized non-adiabatic frequency- and amplitude-modulated pulse (“P”) which fulfills these criteria (16). The shortest element, of course, is a conventional rectangular 180° pulse. However, the very narrow bandwidth and poor compensation for RF inhomogeneity pre-

¹Department of Radiology, Johns Hopkins University School of Medicine, Baltimore, Maryland.

²F.M. Kirby Research Center for Functional Brain Imaging, Kennedy Krieger Institute, Baltimore, Maryland.

³Department of Chemistry, University of California–Irvine, Irvine, California. Grant sponsor: National Science Foundation; Grant number: CHE-9900422.

*Correspondence to: Peter B. Barker, Department of Radiology, MRI 143C, Johns Hopkins University School of Medicine, 600 N. Wolfe St., Baltimore, MD 21287. E-mail: barker@mri.jhu.edu

Received 23 June 2000; revised 31 August 2000; accepted 11 September 2000.

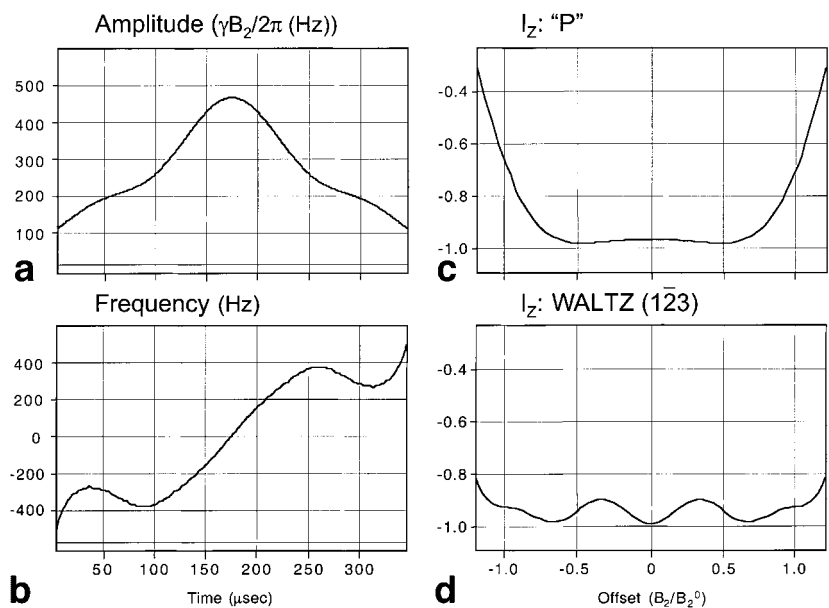
Table 1
Phase (Degrees) and Amplitudes (Arbitrary Units, "1022" Equivalent to 300 Hz ($\gamma B_2/2\pi$)) for a "P" Pulse
With Duration of 3.3 msec (110 Steps, Each Step 30 μ sec)

Phase	Amp	Phase	Amp	Phase	Amp	Phase	Amp
164.70	360.50	68.93	811.00	0.03	1658.37	73.03	792.10
159.97	383.97	64.83	832.17	0.23	1653.43	77.13	775.07
155.37	408.17	60.73	855.77	0.70	1644.13	81.13	759.90
151.20	432.47	56.67	881.70	1.37	1630.13	85.10	746.20
147.40	456.40	52.67	910.13	2.27	1611.37	88.93	733.93
143.83	479.77	48.73	941.30	3.40	1588.63	92.67	722.70
140.50	502.60	44.93	974.87	4.67	1562.17	96.30	711.63
137.23	524.20	41.20	1010.63	6.20	1532.07	99.90	701.17
134.13	544.60	37.60	1048.33	7.90	1498.83	103.33	690.70
131.10	564.23	34.13	1087.80	9.77	1462.77	106.70	679.77
128.10	582.57	30.83	1128.93	11.80	1424.43	109.93	668.37
125.20	599.37	27.67	1171.03	14.07	1384.27	113.07	656.50
122.20	615.70	24.60	1213.83	16.47	1342.63	116.17	643.77
119.20	630.33	21.73	1257.03	19.00	1300.03	119.20	630.33
116.17	643.77	19.00	1300.03	21.73	1257.03	122.20	615.70
113.07	656.50	16.47	1342.63	24.60	1213.83	125.20	599.37
109.93	668.37	14.07	1384.27	27.67	1171.03	128.10	582.57
106.70	679.77	11.80	1424.43	30.83	1128.93	131.10	564.23
103.33	690.70	9.77	1462.77	34.13	1087.80	134.13	544.60
99.90	701.17	7.90	1498.83	37.60	1048.33	137.23	524.20
96.30	711.63	6.20	1532.07	41.20	1010.63	140.50	502.60
92.67	722.70	4.67	1562.17	44.93	974.87	143.83	479.77
88.93	733.93	3.40	1588.63	48.73	941.30	147.40	456.40
85.10	746.20	2.27	1611.37	52.67	910.13	151.20	432.47
81.13	759.90	1.37	1630.13	56.67	881.70	155.37	408.17
77.13	775.07	0.70	1644.13	60.73	855.77	159.97	383.97
73.03	792.10	0.23	1653.43	64.83	832.17	164.70	360.50
		0.03	1658.37	68.93	811.00		

cludes its use. We therefore expanded the pulse length by a factor of 2, and added modulation to improved the off-resonance performance, keeping the root mean square (RMS) power deposition constant. The optimization algorithm and criteria were very similar to those described in Ref. 10. Table 1 provides a listing of amplitudes and phases for the P pulse. Figure 1 shows the inversion profile

of this pulse as a function of frequency offset and also includes the inversion profile of a conventional WALTZ pulse (123) for comparison at the same RMS B_2 level (300 Hz). The WALTZ pulse is 50% longer than the P pulse. The P pulse provides inversion of better quality than the WALTZ pulse over approximately $\pm 0.75B_2$, whereas the WALTZ pulse covers a slightly larger band-

FIG. 1. (a) Amplitude and (b) frequency modulation for the 180° inversion pulse P. The pulse shown has a duration of 3.3 msec, an RMS B_2 field of 300 Hz, and a peak B_2 field of 487 Hz. The inversion profile of this pulse as a function of frequency offset expressed relative to the average B_2 field strength (B_2^0) is shown in c. For comparison, the inversion profile of a WALTZ pulse (123) at the same B_2 level of 300 Hz is also shown (d). Note the superior inversion of the P pulse over a range $\pm 0.75 B_2$, while the WALTZ pulse has poorer inversion over a slightly larger bandwidth ($\pm 1.0 B_2$). The duration of the WALTZ pulse is 50% longer than that of the P pulse.



width ($\pm 1.0B_2$). The inversion performance of P is sufficiently good that the decoupling sequence can consist of just four P elements in an MLEV-4 expansion $PP\bar{P}\bar{P}$, which we abbreviate to PBAR.

Spectra were recorded on a 1.5 T Philips ACS-NT scanner (Philips Medical Systems, Best, The Netherlands) equipped with high performance Powertrak 6000 gradients and dual transmitter channels. For ^{31}P MRS, the Philips quadrature ^{31}P birdcage head coil was used for transmit and receive, and the proton quadrature birdcage body coil was used for broadband decoupling. In vivo spectra were recorded using a sweep width of 1.5 kHz, 1024 data points (682 msec decoupling duration), TR of 5 sec, 128 averages, and a 10-min 40-sec scan time. Volume selection was applied using the ISIS sequence (17) to record an axial slice located at the level of the corpus callosum, voxel size $150 \times 100 \times 40$ mm (600 cm^3) with a nonselective excitation pulse. For ^{13}C , an in-house-built, 11-cm-diameter, two-turn single-tuned (16 MHz) balance-matched surface coil was used for transmit and receive with a nonselective excitation pulse, and a 28-cm-diameter quadrature birdcage (Philips Medical Systems) head coil was used for proton decoupling. The surface coil was positioned inside the head coil closer to the patient table, leaving enough space for the head of the patient. No spatial localization other than that provided by the reception profile of the surface coil was used for ^{13}C studies. In vivo spectra were recorded using a sweep width of 6 kHz, 512 data points (85 msec decoupling duration), TR of 2 sec, and 512 averages for a total scan time of 17 min. Isolation between the ^1H and ^{13}C channels was achieved with 64 MHz high- and 16 MHz low-pass filters, respectively. RF power was monitored both by the Philips system and an inline directional coupler (50 dB) connected to a digital oscilloscope (Tektronix TDS 460, Beaverton, OR). All sequences were within FDA guideline SAR limits of 3.2 W/kg average power deposition for head imaging. Decoupling sequences were started with or without increasing delay times before acquisition. To further suppress cycling sidebands the decoupling sequence was executed with a random delay relative to the start of data acquisition at each scan (asynchronous decoupling). RF power deposition automatically calculated by the Philips scanner was 0.43 W/kg for the head coil.

In addition to the in vivo experiments, tests of the PBAR sequence were also performed on a sample of ^{13}C -enriched formic acid in d6-acetone ($J_{\text{CH}} = 221$ Hz) on a Varian UnityPlus 500 MHz spectrometer equipped with a Varian high-field triple resonance triple axis pulsed field gradient probe. Acquisition parameters are specified in the Fig. 2 legend.

RESULTS

Figure 2a shows the offset dependency of the PBAR and WALTZ-4 sequences on the 500 MHz system at an rms B_2 level of 1 kHz, while Fig. 2b shows the offset dependency of the two sequences at 1.5T on a sample of methanol ($J_{\text{CH}} = 140$ Hz). The rms B_2 level was 500 Hz using 300 W of power into the quadrature head coil. It can be seen that the sequences decouple over the expected range of frequencies based on the pulse inversion profiles, 750 Hz for

PBAR and 1 kHz for WALTZ-4 (with $\gamma B_2/2\pi = 500$ Hz). Note that both sequences decouple a wider range than the normal proton chemical shift range at 1.5T (10 ppm = 640 Hz at 1.5T), but that the cycling sideband intensity is approximately a factor of 3 lower for PBAR than for WALTZ-4 over the effective decoupling range (the maximum decoupling sideband intensity is approximately 6% for PBAR and 18% for WALTZ-4 over ± 750 Hz). Figure 2c shows the sideband pattern under high signal-to-noise conditions on the 500 MHz spectrometer for PBAR and WALTZ-4 on-resonance and at an offset of 100 Hz. At most offsets, PBAR gives sidebands which are smaller by nearly a factor of 2, and no subharmonic sidebands are present within the range ± 250 Hz (i.e., inside the principle harmonic sideband). Other more complex decoupling schemes (such as WALTZ-16) produce a forest of sidebands within a similar range. The sidebands are also spaced further apart in PBAR compared to WALTZ-4, because of the shorter length of the PBAR sequence compared to the WALTZ-4 sequence.

Figure 3 shows ^{31}P spectra from the human brain with and without decoupling using the PBAR sequence. Spectra were recorded with the ISIS localization technique using a quadrature transmit receive birdcage head coil for ^{31}P (provided by Philips) and the Philips quadrature body coil. Decoupled spectra show improved resolution of phosphomonoester and phosphodiester components consistent with previous reports (18). Decoupling is achieved over the large volume of brain tissue (600 cm^3) recorded in this experiment, with the resolution in the downfield region of the spectrum dominated mainly by field inhomogeneity rather than residual scalar couplings.

Figure 4 shows natural abundance ^{13}C spectra from the human head and foot with and without PBAR decoupling. For both organs, the spectrum predominantly consists of glycerol and fatty acid saturated, unsaturated, and carbonyl protons, all of which are successfully decoupled by the PBAR sequence using the quadrature head coil, giving substantial sensitivity improvement over the coupled spectrum without introducing any appreciable sideband intensity.

DISCUSSION

Decoupling sequences for high-resolution NMR have been designed with ever increasing bandwidths for applications at high magnetic fields and/or for decoupling of nuclei with wide chemical shift ranges (9–13). For applications in vivo, comparatively small bandwidths are required for proton decoupling, but only low B_2 field levels are available (particularly for volume head or body coils) at acceptable SAR levels in humans. Therefore, the design criteria for in vivo decoupling sequences are somewhat different from those for high-resolution NMR.

In this work, we describe a custom-designed sequence (PBAR) for in vivo decoupling and optimized for low B_2 levels. As the B_2 level decreases, several factors affect the quality of the decoupling sequence. First, as the length of the sequence increases, the performance of the compensation cycle (in this case the MLEV-4 expansion $PP\bar{P}\bar{P}$) is reduced, particularly if the length of the sequence exceeds $1/J$. Also, for adiabatic decoupling sequences, the perfor-

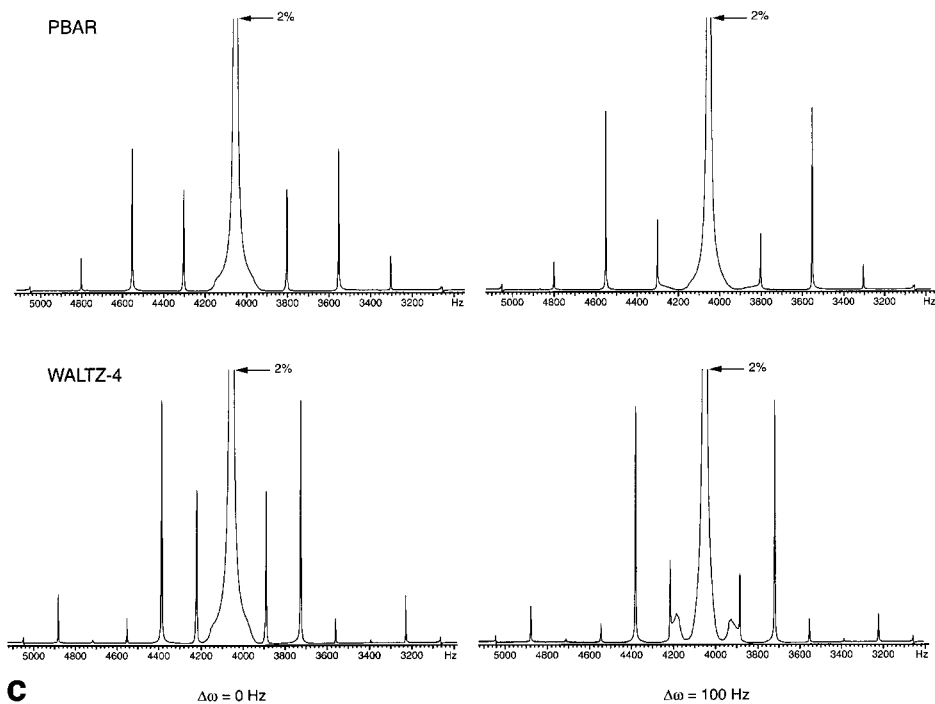
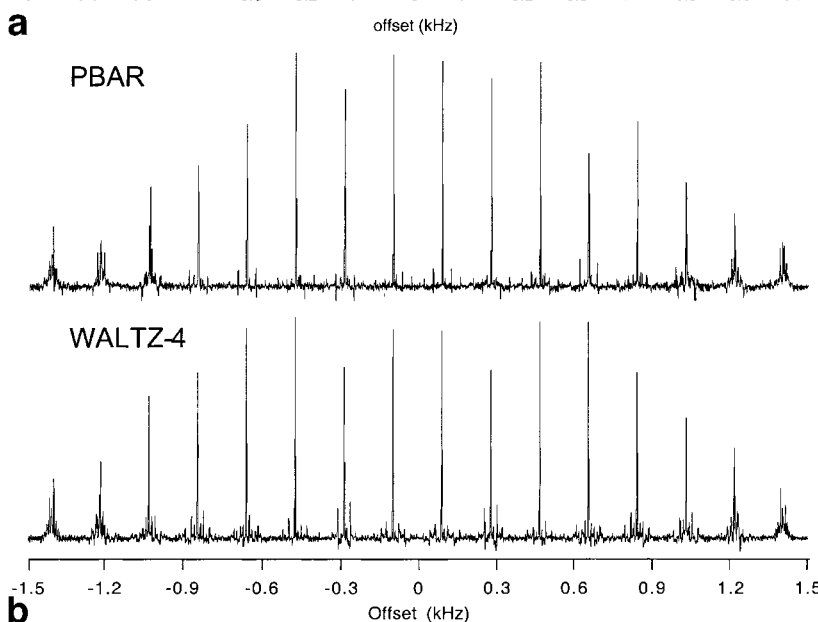
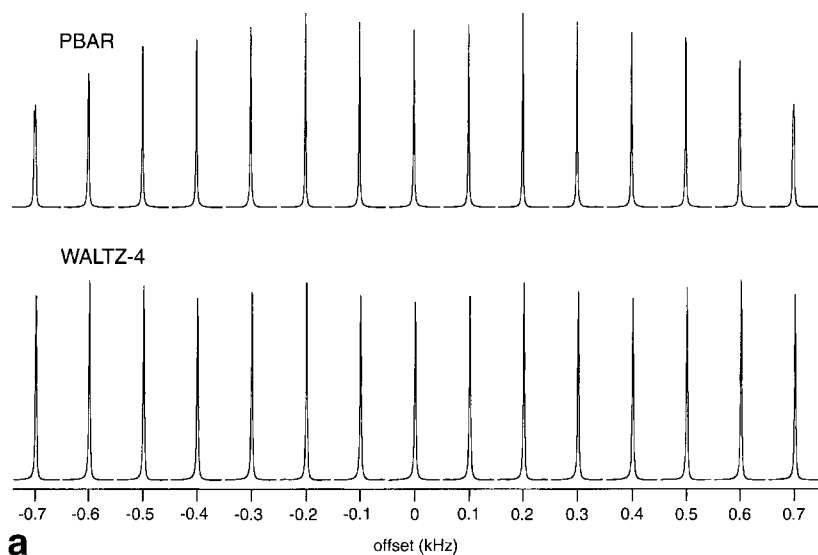


FIG. 2. **a:** Offset dependency of the PBAR and WALTZ-4 sequences in a sample of formic acid ($J_{CH} = 221$ Hz) on the Varian UnityPlus 500 MHz spectrometer. The rms B_2 level was 1 kHz, and the linewidth on-resonance is 3.3 Hz. Spectral width = 5 kHz, TR = 5 sec, and 10000 data points were collected with 4 averages. Note that the peak height of the decoupled resonance is both a function of the scaling factor (λ) and modulation index (i.e., sideband intensity) at each offset. **b:** Offset dependency of the PBAR and WALTZ-4 sequences in a sample of methanol ($J_{CH} = 140$ Hz) on the Philips 1.5T scanner. The rms B_2 level was 500 Hz using 300 W of power into the quadrature head coil. It can be seen that the sequences decouple over the expected range of frequencies based on the pulse inversion profiles: 750 Hz for PBAR and 1 kHz for WALTZ-4. The maximum decoupling sideband intensity is approximately 6% for PBAR and 18% for WALTZ-4 over the decoupling range ± 750 Hz. The linewidth (on-resonance) was 11.7 Hz for both the PBAR and WALTZ-4 sequences (with a 3 Hz exponential filter applied). Spectra are plotted on the same horizontal and vertical scales. **c:** Sideband patterns of the PBAR and WALTZ-4 sequences in a sample of formic acid ($J_{CH} = 221$ Hz) on the Varian UnityPlus 500 MHz spectrometer on-resonance and 100 Hz off-resonance. Spectral width = 100 kHz, TR = 5 seconds, and 100000 data points were collected with 24 averages. The central decoupled line is truncated at 2% of maximum intensity in all spectra. The rms B_2 level was 1 kHz and the linewidth on-resonance is 3.3 Hz. The sideband frequencies are multiples of approximately 250 Hz for PBAR and 166 Hz for WALTZ-4.

c

$\Delta\omega = 0$ Hz

$\Delta\omega = 100$ Hz

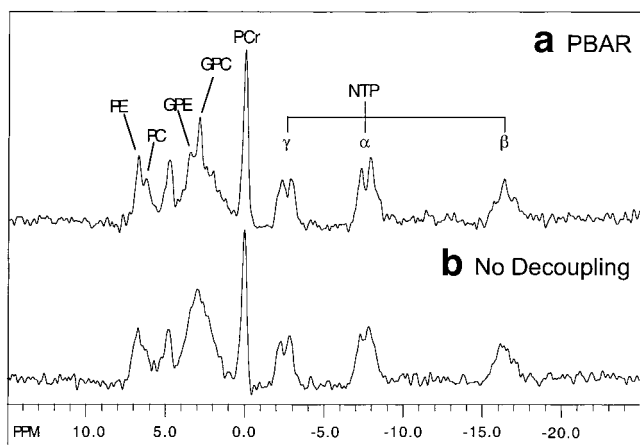


FIG. 3. ^{31}P spectra from the human brain recorded using the ISIS technique (a) with and (b) without PBAR decoupling using the standard body coil of the Philips scanner. Details are provided in text. Note the improved resolution in the phosphomonoester and phosphodiester regions of the spectrum as the result of the removal of the heteronuclear J_{PH} splittings.

mance of the sequence degrades at low B_2 levels when the adiabatic sweep condition $d\theta/dt \ll \omega_{\text{eff}}$ (where $\omega_{\text{eff}} = \sqrt{\Delta\omega^2 + \gamma B_2^2}$, and $\theta = \tan^{-1}(\Delta\omega/\gamma B_2)$) is no longer met. Second, artifacts due to homonuclear couplings increase (19,20). Third, the amplitude of cycling sidebands increases (15). It can be shown that the amplitude of the cycling sidebands increases roughly as $1/B_2^2$ (15). These artifacts can be minimized by designing sequence elements (P) which provide excellent inversion in as short a period of time as possible, under the constraints of acceptable SAR. This criterion is more important than the bandwidth of the pulse (e.g., for decoupling protons at 1.5T bandwidths of less than 600 Hz are required). For this purpose, we chose a frequency swept inversion pulse that provides excellent inversion in 66% of the time of a WALTZ inversion pulse (123). The pulse is non-adiabatic, so it does not require the adiabatic condition to be fulfilled; however, one disadvantage of non-adiabatic pulses is that they will not necessarily work with a wide range of B_2 fields (such as occur with surface coils). Therefore, the PBAR sequence is more suitable for homogeneous head and body volume coils rather than for surface coils. PBAR may be regarded as one out of a whole family of sequences, which may be designed with different amplitude modulation schemes as a function of the required design criteria (16) (bandwidth, pulse length, and acceptable sideband levels).

Several approaches have been described for reducing cycling sidebands by modifying existing decoupling sequences. First, it should be recognized that the phase of some of the sidebands varies depending on the timing of the decoupling sequence relative to the start of data acquisition (15). These sidebands can be eliminated by running the decoupling sequence asynchronously with data acquisition, so that the phase of these sidebands is random from one scan to the next; with time-averaging, the intensity of these sidebands is reduced to near zero. However, this approach does not remove sidebands in which the phase is

coherent with the decoupled resonance regardless of the sequence of timing. These sidebands can be attenuated in several ways. One option is to cyclically permute some element (preferably a small flip angle pulse) of the sequence from one repetition to the next, effectively increasing the length of the sequence and reducing the sideband modulation frequencies (15). If the permutation process is continued throughout the whole of data acquisition, ultimately every data point in the spectrum can contain some sideband intensity. This approach does not reduce the modulation index of the decoupled signal but rather introduces more modulation sidebands, each of which is of lower intensity, thereby decreasing individual sideband intensity. Care should be taken to ensure that decoupling performance is still maintained with these permuted sequences. Other approaches to reducing cycling sideband intensity (which can be large for long sequences, such as adiabatic (3,11–13) sequences or GARP (10)) include modulating the amplitude of the B_2 field (and hence sequence timing (11,21)) or modulating the adiabaticity factor (R) from one repetition of the cycle to the next (22). Again, all of these approaches do not reduce the modulation index of the decoupled line, but rather act to spread out the sidebands, and hence reduce their peak intensity. In adiabatic decoupling, it is also possible to use a time-shifted adiabatic decoupling pulse during the evolution of a spin-echo, which, when combined with a phase-cycle, can eliminate most of the principle sidebands (23). However, the spin-echo approach may not always be feasible in vivo when the detection of short T_2 signals is required.

In the PBAR sequence, we chose a different approach, namely to design a sequence which has short duration and also provides excellent quality of inversion over the fairly narrow range of bandwidths encountered in in vivo spec-

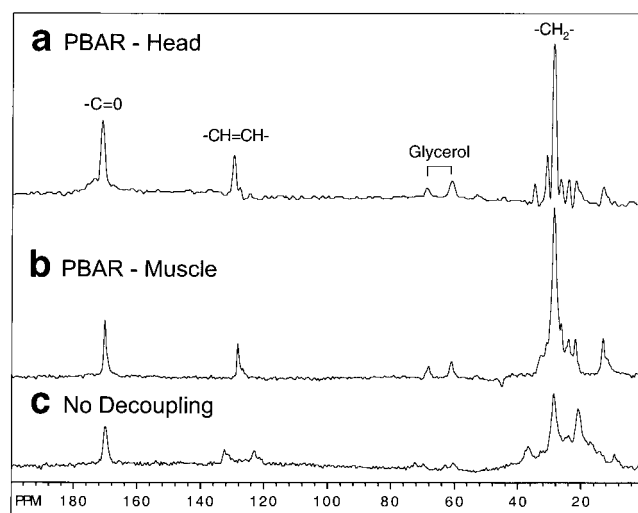


FIG. 4. Natural abundance non-localized surface coil ^{13}C spectra from a human (a) head and (b) foot recorded with PBAR decoupling using the standard Philips quadrature birdcage transmit head coil, and (c) coupled spectrum of the human foot for comparison. Details are provided in text. Decoupled resonances are apparent from carbonyl, saturated and unsaturated lipids resonances, and glycerol. Chemical shift scale relative to tetramethylsilane using the 30.05 ppm fatty acid signal as an internal reference.

troscopy. The better the inversion quality of the individual P pulses, and the briefer their duration, the smaller the sideband intensity since this is the major contributor to the modulation of signal intensity during the decoupling cycle. Reduction of sideband intensity is particularly important in non-localized ^{13}C spectroscopy because of the high dynamic range between the large fatty acid signals and the much smaller metabolite signals. Sidebands from the fatty acid responses could potentially overlap or masquerade as metabolite peaks if decoupling sequences with poor sideband performance are used. Therefore, an additional averaging of cycling sidebands by running the decoupling sequence asynchronously with data acquisition was used for in vivo ^{13}C spectroscopy.

One aspect of amplitude-modulated decoupling schemes is that their peak power level may be appreciably higher than the average power. For the PBAR sequence, the peak power is 2.6 times the average power, and for some RF coil/amplitude configurations it may be difficult to attain these peak power levels either because of limited RF power or coil breakdown at high applied voltages. These sequences also require linear amplifier systems, which generally are available on all modern in vivo imaging/spectroscopy systems since shaped RF pulses are required for slice selection pulses and other applications. Because the dynamic range of PBAR is quite limited, linearity is very unlikely to be a limiting factor in performance.

For in vivo decoupling in humans, RF power monitoring is essential because of the potential heating effects associated with continuous decoupling fields applied during data acquisition. In the current study, power monitoring was performed both by the Philips scanner and also by using an in-line RF signal sampler connected to an oscilloscope next to the operator console. SAR did not exceed the FDA guideline per brain imaging of 3.2 W/kg for head imaging. Using the head coil, for a typical average forward power of 300 W, the SAR is calculated to be 2.125 W/kg based on a duty cycle of approximately 4.25% (85-msec acquisition time and 2-sec TR), an average head mass of 3 kg, and a 50% transfer of RF power (applied to the coil input) to the head (based on measurements of the loaded and unloaded Q-values of the head coil (24)). Induced heating effects in the head are expected to be higher at the surface than in the middle of the sample (25), and temperature monitoring during a 20-min experiment using an external thermocouple did not detect any change in sample temperature from baseline. Because of their location and high conductivity, local heating in the orbits is a potential problem for RF deposition, although currents in the orbits may not be as large as expected because of the relatively low electrical conductivity of retro-orbital fat. No adverse effects from broadband decoupling were reported by any of the volunteers in this study, although this may become a more critical issue when pulse sequences with higher duty cycles are needed. Also, as the blood supply to the brain is an efficient way of regulating cerebral temperature (26), local heating in the brain is unlikely unless patients with regions of low cerebral blood flow (due to stroke or other cerebrovascular disease) are scanned.

In summary, we have described a decoupling sequence for application in vivo with relatively low B_2 decoupling fields. The sequence uses non-adiabatic amplitude- and frequency-modulated pulses that produce good decoupled spectra and have small decoupling artifacts such as cycling sidebands. The sequence was demonstrated in vivo in the human brain for ^{31}P and natural abundance ^{13}C spectroscopy. For the first time, whole-brain $\{^1\text{H}-^{13}\text{C}\}$ decoupling in the human brain is demonstrated using a volume coil. This sequence will therefore allow whole-brain or whole-slice spectroscopic imaging (SI) with $\{^1\text{H}-^{13}\text{C}\}$ decoupling to be performed, an important step in the development of tomographic studies of uptake and metabolism of ^{13}C -labeled substrates in the brain using ^{13}C MRSI. The sequence should also have sufficient bandwidth to be applicable to whole-brain proton decoupling on higher-field (3 or 4T) scanners for in vivo applications in humans.

ACKNOWLEDGMENTS

This work was done during the tenure of an Established Investigatorship from the American Heart Association (P.B.B.). We thank Philips Medical Systems for support, and Dr. Paul Bottomley for helpful discussions. A.J.S. acknowledges the support of the National Science Foundation.

REFERENCES

1. Beckmann N, Turkalj I, Seelig J, Keller U. ^{13}C NMR for the assessment of human brain glucose metabolism in vivo. *Biochemistry* 1991;30: 6362–6366.
2. Gruetter R, Novotny EJ, Boulware SD, Rothman DL, Mason GF, Shulman GI, Shulman R, Tamborlane WV. Direct measurement of brain glucose concentrations in humans by ^{13}C NMR spectroscopy [published erratum appears in *Proc Natl Acad Sci USA* 1992;89:12208]. *Proc Natl Acad Sci USA* 1992;89:1109–1112.
3. Luyten PR, Bruntink G, Sloff FM, Vermeulen JW, van der Heijden JI, den Hollander JA, Heerschap A. Broadband proton decoupling in human ^{31}P NMR spectroscopy. *NMR Biomed* 1989;1:177–183.
4. Bluml S. In vivo quantitation of cerebral metabolite concentrations using natural abundance ^{13}C MRS at 1.5 T. *J Magn Reson* 1999;136: 219–225.
5. Aboagye EO, Bhujwalla ZM. Malignant transformation alters membrane choline phospholipid metabolism of human mammary epithelial cells. *Cancer Res* 1999;59:80–84.
6. Anderson WA, Nelson FA. Removal of residual splitting in nuclear magnetic double resonance. *J Chem Phys* 1963;39:183–189.
7. Ernst RR. Nuclear magnetic double resonance with an incoherent radio-frequency field. *J Chem Phys* 1966;45:3845.
8. Levitt MH, Freeman R, Frenkiel TA. Broadband heteronuclear decoupling. *J Magn Reson* 1982;47:328–332.
9. Shaka AJ, Keeler J, Freeman R. Evaluation of a new broadband decoupling sequence: WALTZ-16. *J Magn Reson* 1983;53:313–340.
10. Shaka AJ, Barker PB, Freeman R. Computer-optimized decoupling scheme for wideband applications and low-level operation. *J Magn Reson* 1985;64:547–552.
11. Starcuk Z, Bartusek K, Starcuk Z. Heteronuclear broadband spin-flip decoupling with adiabatic pulses. *J Magn Reson* 1994;107:24–31.
12. Kupce E, Freeman R. Adiabatic pulses for wideband inversion and broadband decoupling. *J Magn Reson* 1995;115:273–276.
13. Bendall R. Broadband and narrowband spin decoupling using adiabatic spin flips. *J Magn Reson* 1995;112:126–129.

14. Shaka AJ, Keeler J. Broadband spin decoupling in isotropic liquids. *Prog NMR Spect* 1984;19:47–64.
15. Shaka AJ, Barker PB, Freeman R. Cycling sidebands in broadband decoupling. *J Magn Reson* 1986;67:396–401.
16. Smith MA, Shaka AJ. *J Magn Reson* 2001, in press.
17. Ordidge RJ, Connelly A, Lohman JAB. Image-selected in vivo spectroscopy (ISIS). A new technique for spatially selective NMR spectroscopy. *J Magn Reson* 1986;66:283–294.
18. Bluml S, Seymour KJ, Ross BD. Developmental changes in choline- and ethanolamine-containing compounds measured with proton-decoupled (³¹P) MRS in in vivo human brain. *Magn Reson Med* 1999;42:643–654.
19. Barker PB, Shaka AJ, Freeman R. Homonuclear Hartmann-Hahn effects in broadband decoupling. *J Magn Reson* 1985;65:535–539.
20. Shaka AJ, Barker PB, Freeman R. Three-spin effects in broadband decoupling. *J Magn Reson* 1987;71:520–531.
21. Dykstra RW. A method to suppress cycling sidebands in broadband decoupling. *J Magn Reson* 1989;82:347–351.
22. Hwang T-L, Garwood M, Tannus A, van Zijl PCM. Reduction of sideband intensities in adiabatic decoupling using modulation generated through adiabatic R-variation (MGAR). *J Magn Reson* 1996;121:221–226.
23. Kupce E. Effect of sweep direction on sidebands in adiabatic decoupling. *J Magn Reson* 1997;129:219–221.
24. Roschmann P. Radiofrequency penetration and absorption in the human body: limitations to high-field whole-body nuclear magnetic resonance imaging. *Med Phys* 1987;14:922–931.
25. Strilka RJ, Li S, Martin JT, Collins CM, Smith MB. A numerical study of radiofrequency deposition in a spherical phantom using surface coils. *Magn Reson Imaging* 1998;16:787–798.
26. Cabanac M. Selective brain cooling and thermoregulatory set-point. *J Basic Clin Physiol Pharmacol* 1998;9:3–13.